SUPERNOVAE

16.1   A Little History

In 1572 the Danish astronomer Tycho Brahe observed a new star in the constellation of Cassiopeia and described it in his book *De Stella Nova* (Latin for *"Concerning the New Star"*), giving rise to the name *nova*. Novae are now thought to be non-destructive stellar outbursts in one of the members of a binary system (more about this in a subsequent lecture).

In the 1920s, the realisation that many nebulae are located outside the Milky Way Galaxy was taking shape. With the discovery of *A Relation between Distance and Radial Velocity among Extra-Galactic Nebulae* by Edwin Hubble in 1929 (Proceedings of the National Academy of Science, 15, 168), our cosmological horizon expanded significantly.

Only five years later, Baade and Zwicky, working at the Mount Wilson Observatory in southern California, put forward the suggestion that the novae observed in extra-galactic nebulae, the so-called super-novae, were associated with the death of massive stars that produced neutron stars and high energy cosmic rays—a triple correct prediction!

Supernovae are stellar explosions during which the luminosity of a single star quickly reaches 10^9–$10^{10} L_\odot$ and then declines slowly remaining bright for several months. For comparison, the luminosity of the entire Milky Way galaxy is $L_{\mathrm{MW}} \simeq 3 \times 10^{10} L_\odot$, so that a single star which goes supernova can be almost as bright as a whole galaxy for a brief period of time. This makes them ideal candidates for searches by amateur astronomers, as they can easily be spotted with even modest aperture telescopes. Nowadays, hundreds are discovered every year thanks to automatic searches using robotic telescopes. SNe are named with the year of discovery followed by letters; thus, SN2010A through to SN2010Z, followed by SN2010aa through to SN2010az, followed by SN2010ba, and so on, in chronological order of discovery.

16.2   Supernova Remnants

From the rate at which supernovae occur in external galaxies, it has been estimated that the SN rate in our own Galaxy is in the range 2–3 SNe per century. Even allowing for the fact that only about half of the Galaxy may be visible from the Sun's location (we cannot readily see stars on the opposite side of the Galactic bulge), it appears that we are 'overdue' a SN, since the last recorded Galactic supernova exploded in 1604, four years before the invention of the telescope and six years before the italian astronomer Galileo pointed his home-made telescope at Jupiter and discovered its four main satellites. In other words, there has not been a visible Galactic supernova since the birth of modern astronomy.

Table 16.1. Historical supernovae.

year (AD)	V (peak)	SN remnant	SN type	compact object
185	−2	RCW 86	Ia?	–
386		?	?	
393	−3	?	?	
1006	−9	PKS 1459-41	Ia?	–
1054	−6	Crab nebula	II	NS (pulsar)
1181	−1	3C 58	II	NS (pulsar)
1572	−4	'Tycho'	Ia	–
1604	−3	'Kepler'	Ia?	–
~1667	$\gtrsim$+6	Cas A	IIb	NS

However, at least eight Galactic supernovae have been recorded over the past 2000 years by Chinese and in some cases also by Japanese, Korean, Arabian and European astronomers (see Table 16.1). The remnants of these supernovae are in most cases still visible as luminous expanding nebulae, containing the matter that was expelled in the explosion. Supernova remnants (SNRs) remain observable at optical, radio and X-ray wavelengths for tens of thousands of years, as the stellar ejecta interact with the ambient interstellar medium (see Figure 16.1). David Green's catalogue of Galactic SNRs (http://www.mrao.cam.ac.uk/surveys/snrs/) lists 310 entries.

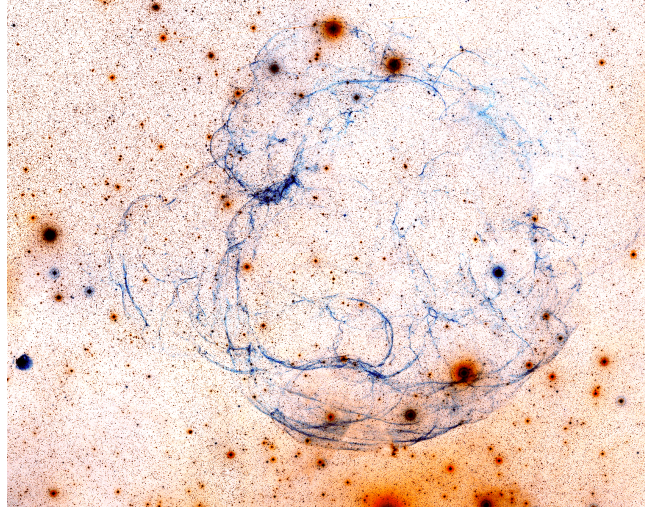Figure 16.1: Image of the faint supernova remnant Simeis 147. This Type II supernova exploded ∼ 100 000 years ago, leaving behind a spinning neutron star or pulsar. Its remnant now extends over nearly three degrees on the sky in the constellation of Taurus.

16.3   Classification of Supernovae

A number of different evolutionary paths can lead to a supernova explosion. Before these paths became understood (and indeed there is still considerable uncertainty regarding some of them, as we shall see presently), an empirical classification for supernovae was developed, based on two observables: (i) their spectra, and (ii) their light curves, by which we mean the way their luminosity decays with time following maximum light. Figure 16.2 summarises the main SN types.
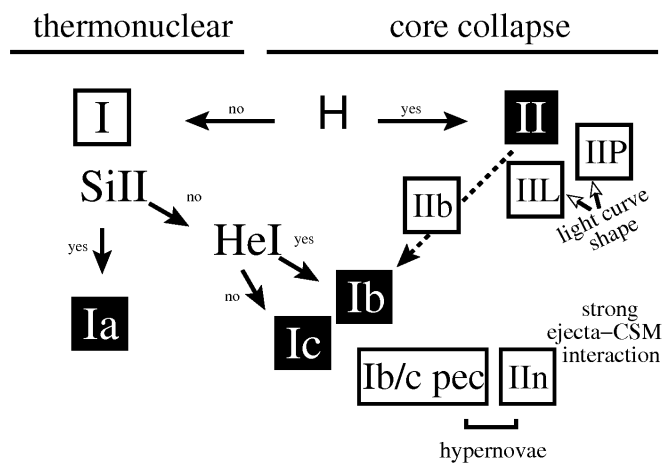

Figure 16.2: Spectral classification of supernovae, based on their spectra and light curve shapes. The main SN types are shown as black squares. (Figure reproduced from Turatto 2003, LNP, 598, 21).
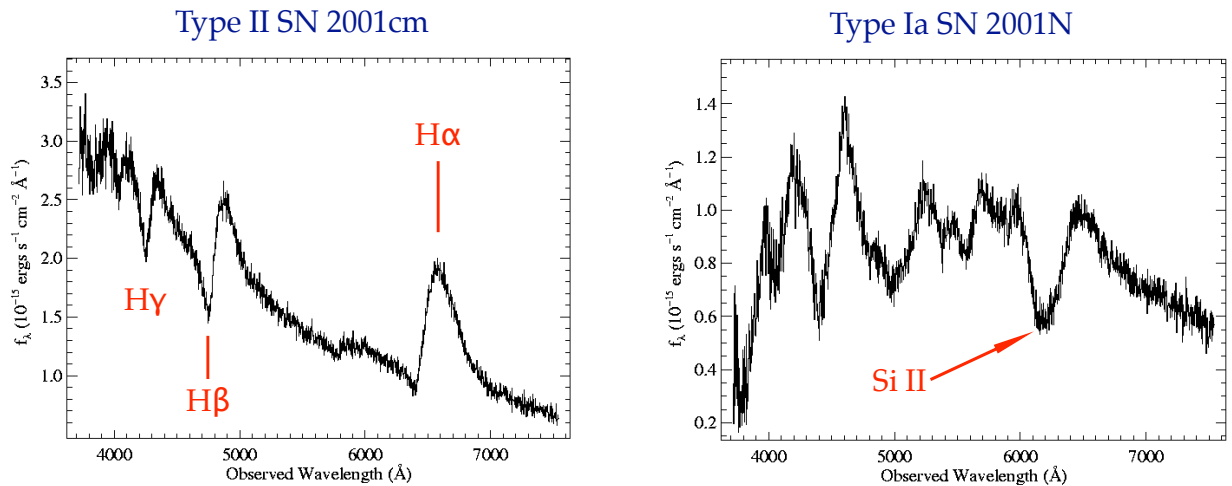
Figure 16.3: Typical optical spectra of Type II and Type Ia supernovae. (Spectra retrieved from www.supernovae.net).

SNe are divided between Type II and Type I depending on whether their optical spectra (usually at peak luminosity) exhibit hydrogen lines or not (see Figure 16.3). Supernovae of Type I are further subdivided into Type Ia if they show a prominent Si II $\lambda 6355$ absorption line, as in Figure 16.3, and Types Ib/Ic if they don't. Types Ib and Ic are differentiated on the basis of the presence or absence of He I lines. Type II SNe are labelled Type II-P (the more common type) and Type II-L depending on whether their light curves exhibit a plateau or a linear decay (see Figure 16.4).

A further distinction between Type Ia and other SNe is their location within a galaxy. Type Ia occur in galaxies of all types, and are the only SNe to occur in elliptical galaxies; since ellipticals have old stellar populations,
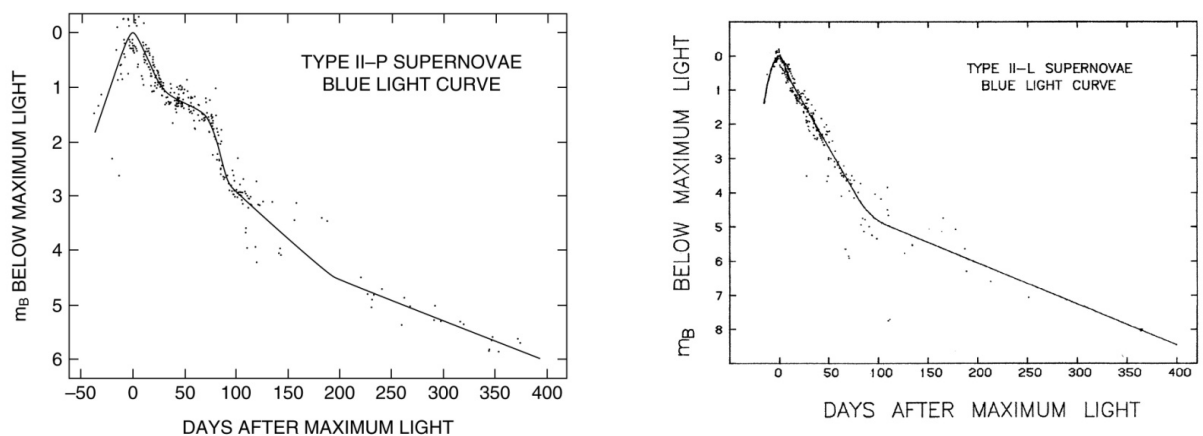

Figure 16.4: Typical light curves of Type II supernovae, from photometric m_B measurements of many Type II-P and Type II-L events. (Figures reproduced from Doggett & Branch 1985, AJ, 90, 2303).

4

this observation suggests that Type Ia SNe can have long-lived, low-mass progenitors. In contrast, Types II, Ib and Ic are associated with regions of star formation in spiral galaxies, and therefore are likely to have short-lived, high-mass progenitors. These observations have led to the current view that:

(1) Type Ia are caused by the thermonuclear explosion of a CO white dwarf as a result of mass accretion in a binary system. About 25–30% of supernovae are of Type Ia. They are (on average) the most luminous of all supernova types and their light curves form a rather homogeneous group; the combination of these two characteristics makes them the best standard candles over cosmological distances. We shall return to Type Ia supernovae in a subsequent lecture.

(2) Types II, Ib, and Ic SNe are collectively referred to as *core-collapse* supernovae, and are thought to be the end stage in the evolution of massive stars. While the progenitors of Type II SNe are still surrounded by a massive H-rich envelope when they explode, Type Ib progenitors have lost their H-rich envelope and Type Ic progenitors have also lost most of their He layer surrounding the core prior to the SN explosion. This sequence can be a consequence of mass loss from stars of increasing initial mass, as we saw in Lecture 15, but can also result from interaction with a binary companion. The remainder of this lecture is concerned with core-collapse supernovae.

16.3.1   The Progenitors of Core-Collapse Supernovae

Since the launch of the *Hubble Space Telescope* in 1990, a public-access archive of high resolution images of nearby galaxies has been accumulating. With high-precision astrometry, it has become possible to search for the progenitors of recent core-collapse supernovae in pre-supernova images of the host galaxies. This is fundamental work, providing empirical tests of our theories of stellar evolution for massive stars. Two teams, one based at Queen's University, Belfast and the other at the University of California, Santa Cruz, have been particularly active in such endeavours; an excellent review of their results up to 2008 is given by Smartt, S. J., 2009, ARAA, 47, 63. Figure 16.5 shows three examples of nearby Type II-P SNe with unambiguous red supergiant progenitors.
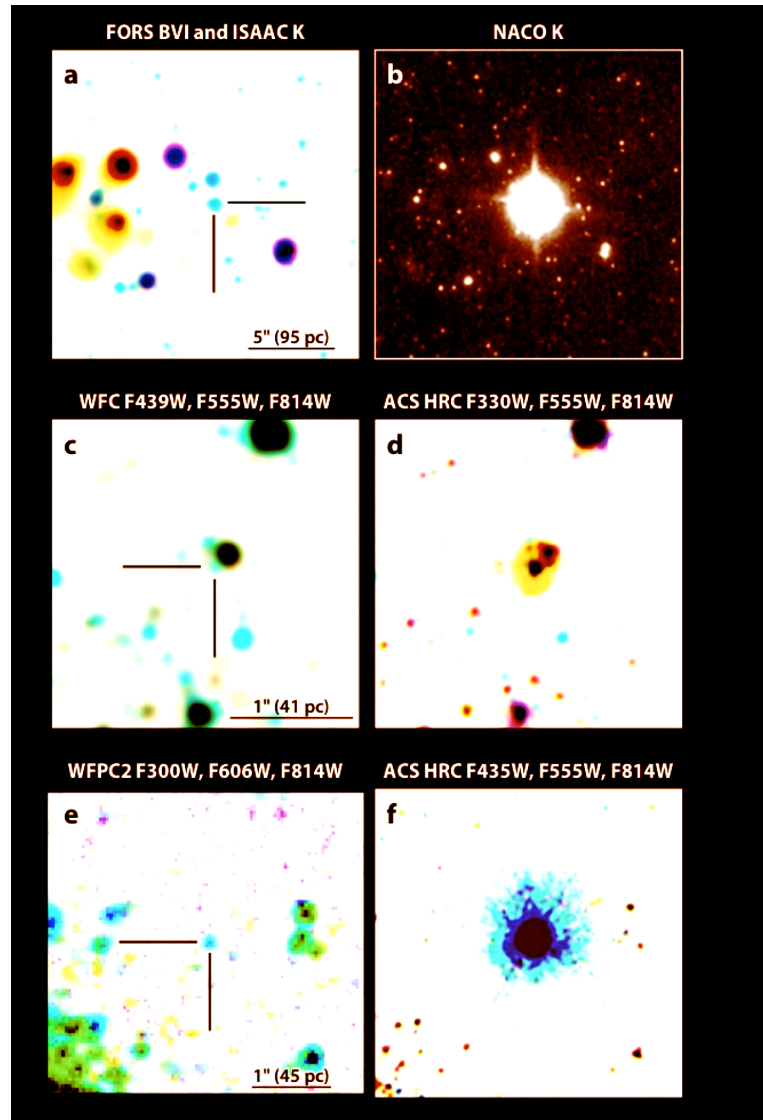
Figure 16.5: Hunting for SN progenitors. The left images show unambiguous red supergiants at the exact locations of subsequent Type II-P supernovae. *Top pair*: SN2008bk in the Scd spiral NGC7793 at a distance of $\sim 4\,\mathrm{Mpc}$. *Middle pair*: SN2005cs in M51 at a distance of $\sim 7\,\mathrm{Mpc}$. *Bottom pair*: SN2003gd in the face-on spiral galaxy M74 at a distance of $\sim 9\,\mathrm{Mpc}$. (Figure reproduced from Smartt 2009, ARAA, 47, 63).

Figure 16.6 summarises our current 'best' picture of the evolutionary paths to different core-collapse supernovae. The search for SN progenitors has produced a number of surprises, as well as confirming some aspects of the accepted scenario for the evolution of massive stars. As expected, red supergiants are the likely progenitors of most Type II-P SNe, but this channel seem to operate only for a relatively narrow mass range, for stars with initial masses between $M_{\mathrm{min}} = 8.5^{+1}_{-1.5} M_\odot$ and $M_{\mathrm{max}} = 16.5 \pm 1.5 M_\odot$. While the lower limit conforms to our ideas of the mass required to ignite carbon and heavier elements in the stellar core, as discussed in Lecture

8 – 17 $M_\odot$ | BIV–O9.5V main-sequence

Slow to moderate rotation → RSG → II-P SN → NS
Fast rotation → BSG → SN1987A → NS
→ Interacting binary → IIb → NS
→ Ibc → NS

17 – 30 $M_\odot$ | O9.5V–O6V

Slow to moderate rotation → RSG → Faint SN? → BH
Fast rotation → WR star → Broad-lined Ibc → NS or BH?
→ Interacting binary → Ibc or faint SN? → NS / BH

>30 $M_\odot$ | O6V–O3V

Slow to moderate rotation → WR → Faint SN? → BH
Fast rotation → WR → Broad-lined Ibc → BH
→ GRB at low-Z → BH
→ LBV → Ultrabright SNe → PISN or Jet?
→ IIn → PISN or Jet?
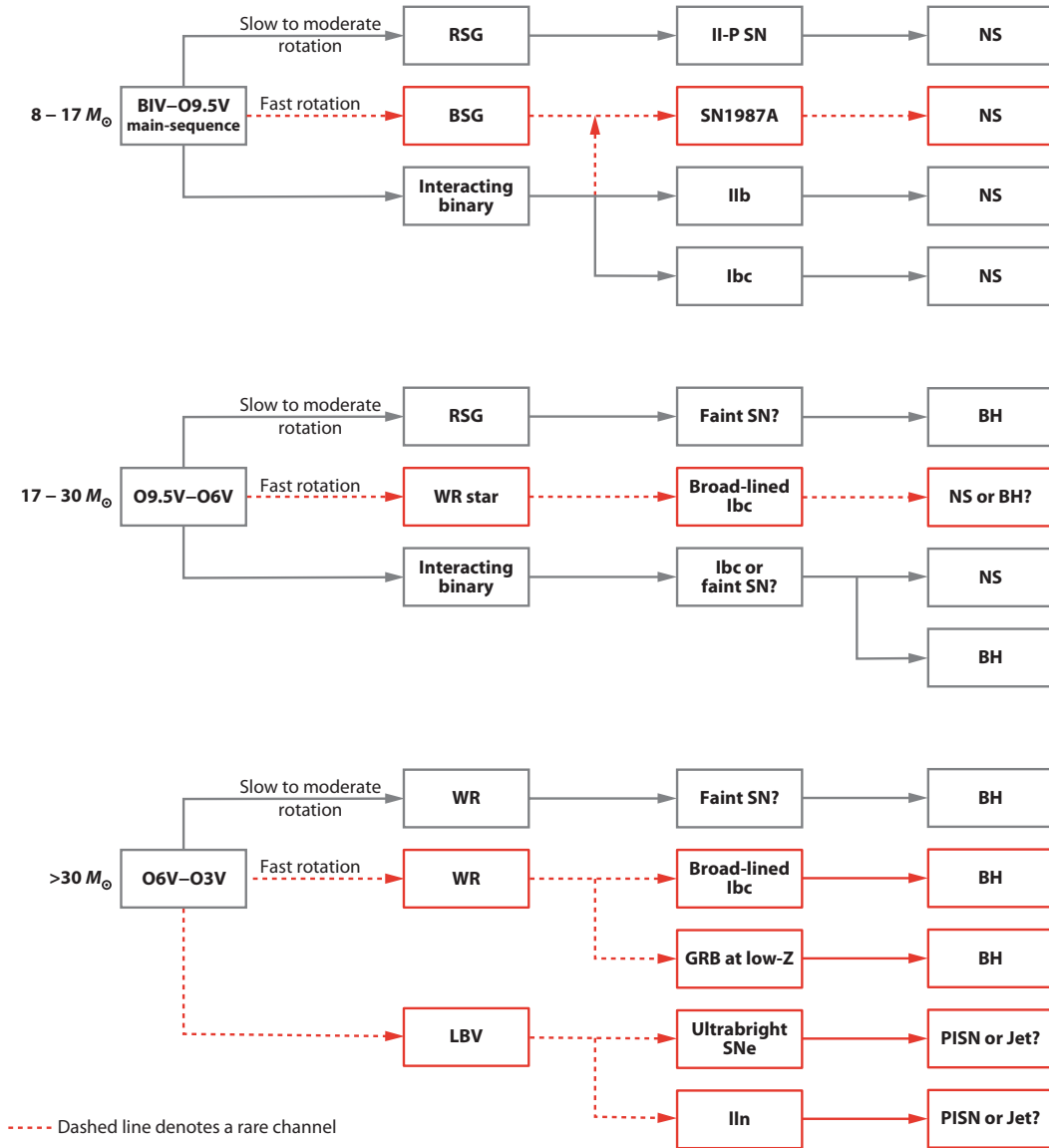
----- Dashed line denotes a rare channel

Figure 16.6: Summary diagram of possible evolutionary pathways and end states of massive stars—constructed on the basis of current empirical evidence and theoretical ideas—and illustrating the probable diversity in evolution and explosion. It is likely that metallicity, binarity and rotation all play important roles in determining the end states. The acronyms are for neutron star (NS), black hole (BH), and pair-instability supernova (PISN). Rare channels of evolution are shown with dashed lines. The 'faint supernovae' have been proposed but not yet detected. (Reproduced from Smartt 2009, ARAA, 47, 63).

15.1, the lack of SNe from RSG progenitors with initial masses between 17 and $30 M_\odot$ was unexpected. And yet, with detections (or upper limits) for 45 supernova progenitors, it now seems well established that there is a deficit of high luminosity stars exploding as core-collapse supernovae (see Figure 16.7).
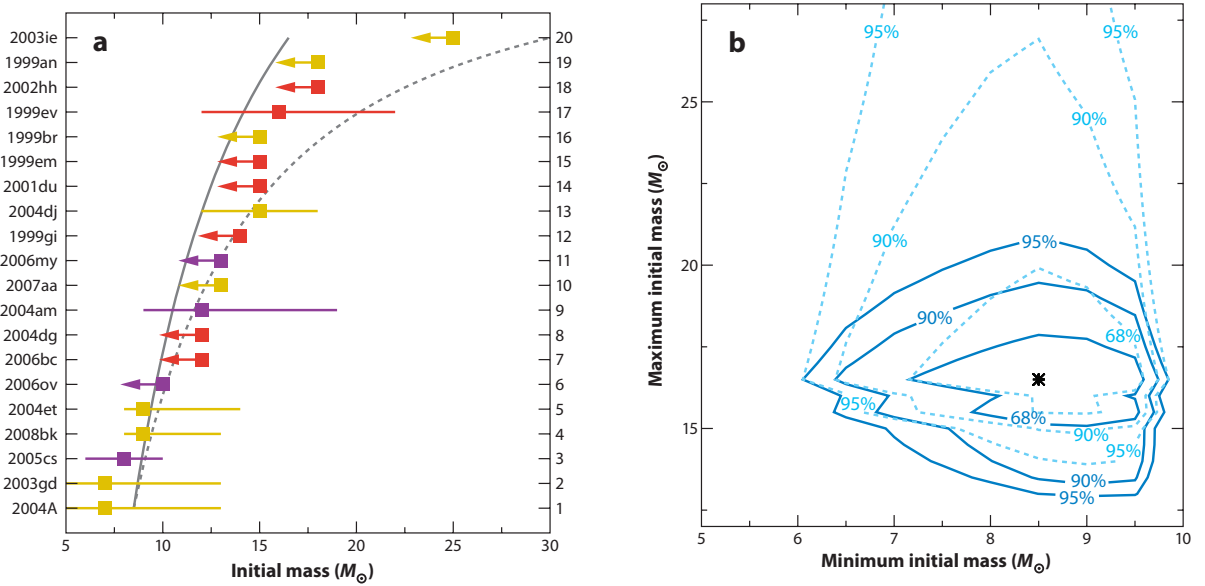
Figure 16.7: *Left:* Cumulative frequency plot of the masses of SN Type II-P progenitors, in order of increasing mass. The solid curve is a Salpeter Initial Mass Function with slope $\alpha = 2.35$ (Lecture 11.9) between $M_{\min} = 8.5 M_\odot$ and $M_{\max} = 16.5 M_\odot$, which gives the most likely fit to the data. The dotted line is also a Salpeter IMF, but with $M_{\max} = 30 M_\odot$, showing that such massive progenitors should have been detected by now, if they gave rise to Type II SNe. The supernovae have been colour-coded according to the metallicity of the parent galaxy. *Right:* Maximum likelihood analysis of the Type II-P progenitor sample gives the most likely values for $M_{\min}$ and $M_{\max}$ (star symbol) and the likelihood contours, calculated for the detections only (dashed lines) and including the upper limits to the progenitor mass (solid lines). (Both figures reproduced from Smartt 2009, ARAA, 47, 63; see also a more recent update with improved statistics in Smartt 2015, PASA, 32, e016).

While several factors, including metallicity effects, variable IMF, dust obscuration, explosions as the rarer II-L, IIn, and Ibc SNe could all be possible explanations, the most intriguing possibility is that stars more massive than $\sim 18 M_\odot$ may collapse 'quietly' to form black holes and either very faint supernovae or no supernova at all. The existence of black holes with masses $M_{\rm bh} > 20 M_\odot$ has now been confirmed by the detection of gravitational waves from merging black-hole binaries.

Furthermore, it is almost certain that interacting binaries play an important role in determining the relative rates of types within SN populations. At the same time, there are indications that different channels can produce similar SNe, with examples of both an interacting binary (SN1993J) and a single WN star (SN2008ax) exploding as Types IIb— which are SNe whose initial spectra show some H, but then quickly evolve into Type Ib (Figure 16.2). However, so far there is no empirical confirmation that mas-

sive Wolf-Rayet stars produce the majority of Ibc SNe in the local Universe. Undoubtedly, the schematic diagram in Figure 16.6 will become clearer as the work to identify SN progenitors continues.

16.4 Core Collapse

Despite the fact that different evolutionary paths can lead to a core-collapse supernova, the physical mechanism that produces the explosion is thought to be essentially similar for Type II, Ib and Ic SNe. As we saw in Lecture 15, by the end of its life a star with $M \gtrsim 11 M_\odot$ has developed an iron core. When the iron core in the centre of a massive star grows, by silicon shell burning, to a mass around the Chandrasekhar mass limit of $\sim 1.44 M_\odot$, electron degeneracy pressure can no longer stabilize the core. Unable to generate additional energy through nuclear fusion, the core collapses from an initial radius $R_{c,i} \sim 3000 \, \text{km}$ to a final radius of only $R_{c,f} \sim 20 \, \text{km}$ (from the size of the Earth to the size of Manchester!) on a very short timescale, of order of a fraction of a second. This starts what is called a core-collapse supernova, in the course of which the star explodes and parts of the star's heavy-element core and of its outer shells are ejected into the interstellar medium.

16.4.1 Energetics

Before considering further the details of core-collapse and the subsequent supernova explosion, let us calculate the energies involved. From the virial theorem, the gravitational energy released by the core collapse is:

$$U_{\text{gr}} = -\frac{3}{10} \frac{GM_c^2}{R_{c,i}} + \frac{3}{10} \frac{GM_c^2}{R_{c,f}} \simeq \frac{3}{10} \frac{GM_c^2}{R_{c,f}} \tag{16.1}$$

since $R_{c,i} \gg R_{c,f}$. With $R_{c,f} = 20 \, \text{km}$ and $M_c = 1.4 M_\odot$, we have:

$$U_{\text{gr}} = \frac{3}{10} \frac{6.7 \times 10^{-11} \left(1.4 \times 2 \times 10^{30}\right)^2}{2 \times 10^4} \quad \frac{\text{m}^3 \, \text{kg}^{-1} \, \text{s}^{-2} \, \text{kg}^2}{\text{m}} \tag{16.2}$$

$$U_{\text{gr}} = \frac{3}{10} \frac{6.7 \times 10^{-11} \left(2.8\right)^2 \times 10^{60}}{2 \times 10^4} \quad \text{kg} \, \text{m}^2 \, \text{s}^{-2} \tag{16.3}$$

$$U_{\mathrm{gr}} = \frac{3}{10} \times 2.6 \times 10^{45} \sim 1 \times 10^{46}\,\mathrm{J} \sim 1 \times 10^{53}\,\mathrm{erg} \qquad (16.4)$$

For comparison, the gravitational binding energy of the rest of the star (the envelope) is:

$$U_{\mathrm{env}} = -4\pi G \int_{R_{\mathrm{c,i}}}^{R_{\mathrm{env}}} M_r\,\rho\,r\,dr \qquad (16.5)$$

where M_r is the mass internal to r, and the integration is carried out from the bottom of the envelope to the stellar radius (eq. 7.6). Integrating eq. 16.5 with an appropriate density distribution $\rho = f(r)$, yields $E_{\mathrm{env}} \sim 10^{50}\,\mathrm{erg}$ as the energy required to unbind the star.

As we have seen (section 16.2), a supernova explosion doesn't just unbind the star, but also ejects its outer layers into the surrounding interstellar medium at high speeds. Typical values for Type II SNe are $M_{\mathrm{ej}} \sim 10 M_\odot$ and $\langle v_{\mathrm{ej}} \rangle \sim 3 \times 10^3\,\mathrm{km\,s^{-1}}$. Thus,

$$E_{\mathrm{ej}} \sim \frac{1}{2} 10 \times 2 \times 10^{30} \cdot \left(3 \times 10^6\right)^2 \qquad \mathrm{kg\,m^2\,s^{-2}} \qquad (16.6)$$

or $E_{\mathrm{ej}} \sim 10^{44}\,\mathrm{J} \equiv 10^{51}\,\mathrm{erg}$.

Finally, a Type II SN has a mean bolometric luminosity $\langle L_{\mathrm{bol}} \rangle \sim 2 \times 10^8 L_\odot$ over a period of several months. Thus, the total energy lost as radiation is:

$$E_{\mathrm{ph}} \sim 2 \times 10^8 \times 4 \times 10^{26} \cdot 100 \times 10^5 \qquad \mathrm{J\,s^{-1}\,s} \qquad (16.7)$$

or $E_{\mathrm{ph}} \sim 10^{42}\,\mathrm{J} \equiv 10^{49}\,\mathrm{erg}$.

Summarising, $E_{\mathrm{env}} + E_{\mathrm{ej}} + E_{\mathrm{ph}} \sim 10^{51} \simeq 0.01\,U_{\mathrm{gr}}$: only about 1% of the energy released in the final collapse of the iron core is used in the supernova event. However, the exact details of how this 1% of the gravitational energy is actually converted into the kinetic energy of the envelope—that is the actual mechanics of the explosion of a massive star—turns out to be a very difficult problem that has been the subject of intense theoretical activity in the modern computational era.

16.4.2   The Explosion Mechanism

At the high temperatures required for Si burning, $T \gtrsim 3 \times 10^9\,\mathrm{K}$, the photon energies are so high ($h\nu \sim 1\,\mathrm{MeV}$) that photons can photodisintegrate iron

nuclei, e.g.:

$$_{26}^{56}\text{Fe} + \gamma \rightarrow 13\,_2^4\text{He} + 4\text{n}$$
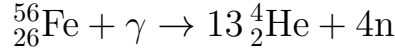
This process takes energy away from the radiation field and reduces the pressure supporting the core; the core contracts, increasing the local temperature further, until photons are sufficiently energetic to photodisintegrate He nuclei:

$$_2^4\text{He} + \gamma \rightarrow 2\text{p}^+ + 2\text{n}$$
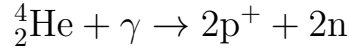
At this point, the core of the star is composed mainly of protons, neutrons and free electrons. As the core continues to collapse, the densities become so large that free electrons are captured by the protons produced by photodisintegration in an inverse β decay:

$$\text{p}^+ + \text{e}^- \rightarrow \text{n} + \nu_\text{e}$$
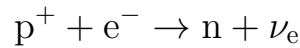
The removal of electrons from the plasma removes another source of pressure: the degeneracy pressure of free electrons. Without energy support the core collapses catastrophically on a timescale of milliseconds until the
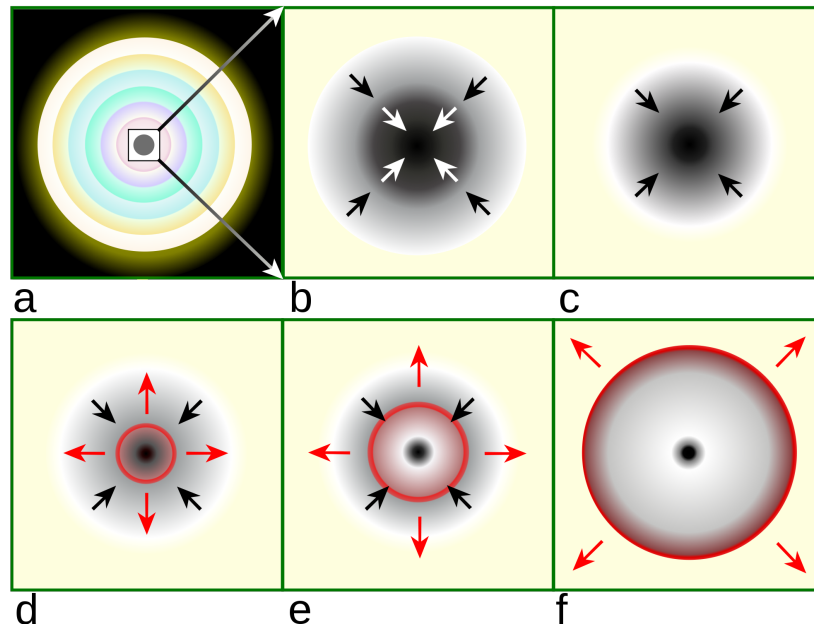

Figure 16.8: Within a massive, evolved star (a) the onion-layered shells of elements undergo fusion, forming an iron core. (b) Unable to generate energy by further fusion, the iron core starts to collapse. The inner part of the core is compressed into neutrons (c), causing infalling material to bounce (d) and form an outward-propagating shock front (red). The shock starts to stall (e), but it is re-invigorated by a process that may include neutrino interaction. The surrounding material is blasted away (f), leaving only a degenerate remnant.

density in the inner core reaches values comparable to the density of matter inside atomic nuclei ($\rho_{\mathrm{nuc}} \simeq 3 \times 10^{14}\,\mathrm{g\ cm^{-3}}$).

The neutralisation of the plasma via the inverse β-decay is also thought to occur in stars with masses $8M_\odot \lesssim M \lesssim 11M_\odot$ which develop degenerate O-Ne cores, rather than Fe cores. The removal of the electron degeneracy pressure results in the core collapsing on the very short dynamical timescale, similar to the mechanism just described for stars with $M \gtrsim 11M_\odot$. This explains the lower limit $M_{\mathrm{min}} \simeq 8M_\odot$ for the progenitors of Type II SNe.

When the density in the inner core increases beyond nuclear densities, the neutrons (which are also fermions) become degenerate resulting in a strong increase in pressure which reverses the collapse. Almost instantaneously, the core becomes incompressible and bounces back like a spring—an event named 'core bounce'.

As the velocity of the inner core material is reversed, it encounters matter from the outer part of the core which is still in free-fall. This creates a shock wave that propagates into the outer layers of the star. The kinetic energy stored in the shock wave was once thought to be sufficient to blow off the envelope, giving rise to a so-called 'prompt explosion'. However, as the shock wave travels through the infalling matter which still mostly consists of iron group nuclei, it heats up the nuclei and disintegrates them effectively into protons and neutrons. Computer simulations indicate that, at this point, the shock stalls.

After the core bounce, a compact remnant begins to form at the centre

Stage	Core temperature (K)	Core density (kg/m³)	Duration of stage
Hydrogen burning	4×10^7	5×10^3	7×10^6 years
Helium burning	2×10^8	7×10^5	7×10^5 years
Carbon burning	6×10^8	2×10^8	600 years
Neon burning	1.2×10^9	4×10^9	1 year
Oxygen burning	1.5×10^9	10^{10}	6 months
Silicon burning	2.7×10^9	3×10^{10}	1 day
Core collapse	5.4×10^9	3×10^{12}	¼ second
Core bounce	2.3×10^{10}	4×10^{15}	milliseconds
Explosive (supernova)	about 10^9	varies	10 seconds

Figure 16.9: Evolutionary stages of a $25M_\odot$ star.

of the collapsing star, rapidly growing by the accretion of infalling stellar material until the explosion sets in. This nascent remnant—the proto-neutron star—will evolve into a neutron star or may eventually collapse to a black hole, depending on whether the progenitor star had a mass below or above $\sim 25 M_\odot$.

Much computational work has focussed on the so-called 'neutrino-driven' explosion (see Figure 16.10). Neutrinos are trapped within the proto-neutron star because the density of matter is so high that their mean free path is significantly shorter than the radius of the neutron star and they take a fraction of a second to diffuse out. In the explosion scenario by the 'delayed neutrino-heating mechanism', the stalled shock wave can be revived by neutrinos depositing some of their energy in the layers between the nascent neutron star and the stalled shock front, mainly by charged-current ν_e and $\bar{\nu}_e$ captures on free nucleons:

$$\nu_e + n \to e^- + p$$

and

$$\bar{\nu}_e + p \to e^+ + n$$

This neutrino heating increases the pressure behind the shock and the heated layers begin to expand, creating between the shock front and the neutron star surface a region of low density but rather high temperature, the so-called 'hot bubble'. The persistent energy input by neutrinos keeps the pressure high in this region and drives the shock outwards again, eventually leading to a supernova explosion (bottom panels of Figure 16.10). This may take a few $100\,\mathrm{ms}$ and requires that during this time interval a few percent of the neutrino energy is converted into thermal energy of nucleons, leptons and photons.

Other recent work has proposed a novel idea: the excitation of core pulsation modes in the deep interior of the proto-NS. The sound pulses radiated from the core steepen into shock waves that merge as they propagate into the outer mantle, depositing their energy and momentum. The ultimate source of the acoustic power is (as in other scenarios) the gravitational energy of infall—core oscillation acts like a transducer to convert this accretion energy into sound. An advantage of the acoustic mechanism is that acoustic power does not abate until accretion subsides, so that it is available as long as it may be needed to explode the star.
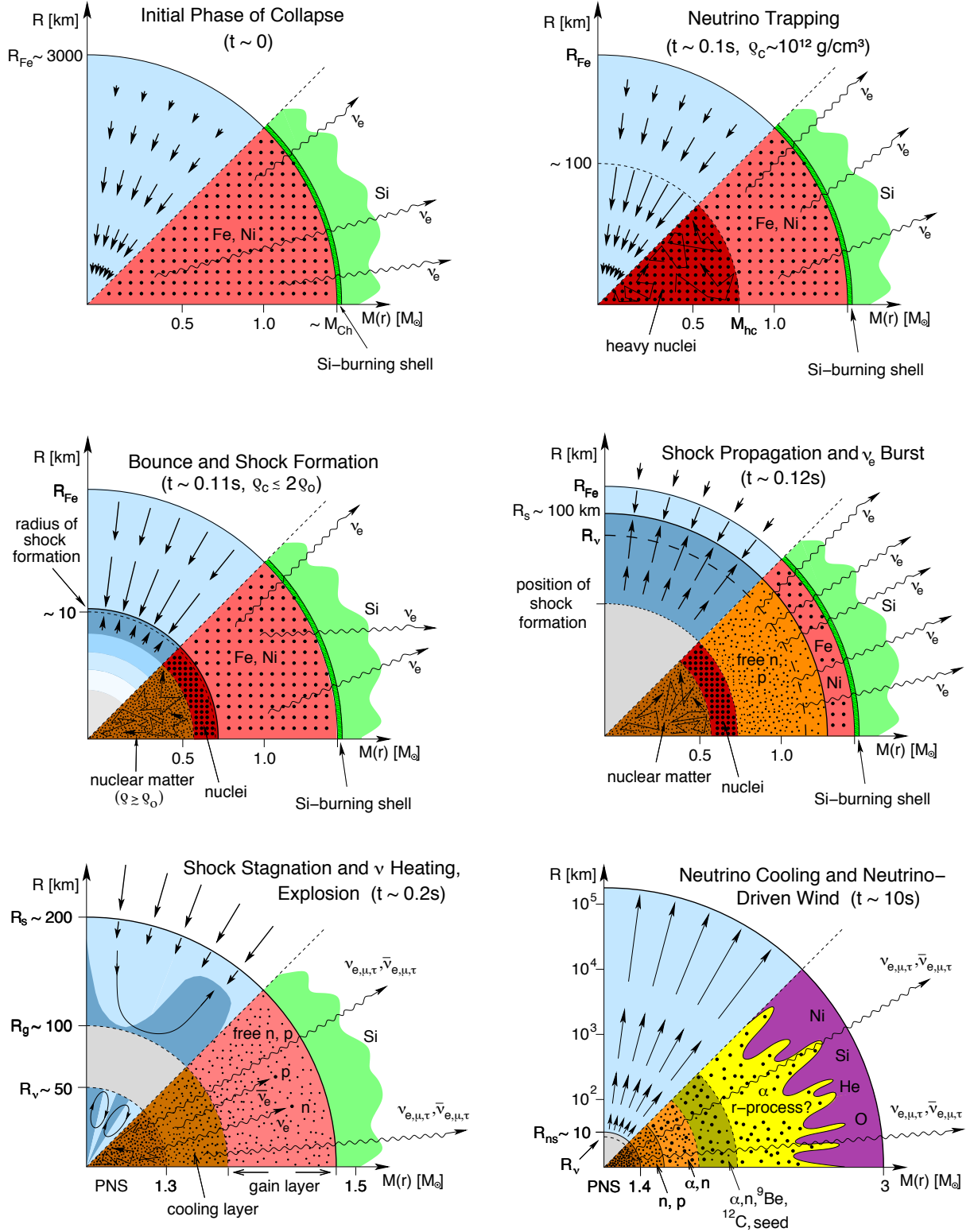
Figure 16.10: Computer simulations of the 'delayed neutrino-heating mechanism' driving Type II supernova explosions. The panels display the dynamical conditions in their upper half, with arrows representing velocity vectors. The nuclear composition, as well as the nuclear and weak processes, are indicated in the lower half of each panel. The horizontal axis gives mass information. (Figure reproduced from Janka et al. 2007, Physics Reports, 442, 38).

It may well be that some supernovae explode by the neutrino mechanism, while others, if the neutrino mechanism fizzles, explode by the acoustic mechanism. Or maybe neither works! Whatever the mechanism, it is clear that massive stars do explode as SNe. In computer simulations of Type II SN explosions, our lack of knowledge of the explosion mechanism is circumvented by introducing by hand a 'piston'—an injection of a specified amount of energy that drives the explosion—so that its consequences can be followed numerically. Both E_{kin} and the mass boundary between core and envelope (usualy referred to as the 'mass cut') are uncertain and are usually treated as free parameters. While ultimately disappointing, this type of 'fudge' is not uncommon in numerical simulations of astrophysical processes.

16.5   Explosive Nucleosynthesis

The photodisintegration and inverse β-decay reactions which take place during core collapse and the shock expansion following core bounce all produce free neutrons. Neutrons do not experience a Coulomb barrier, so that they can be incorporated more easily than charged particles into Fe-peak nuclei to form heavier elements.
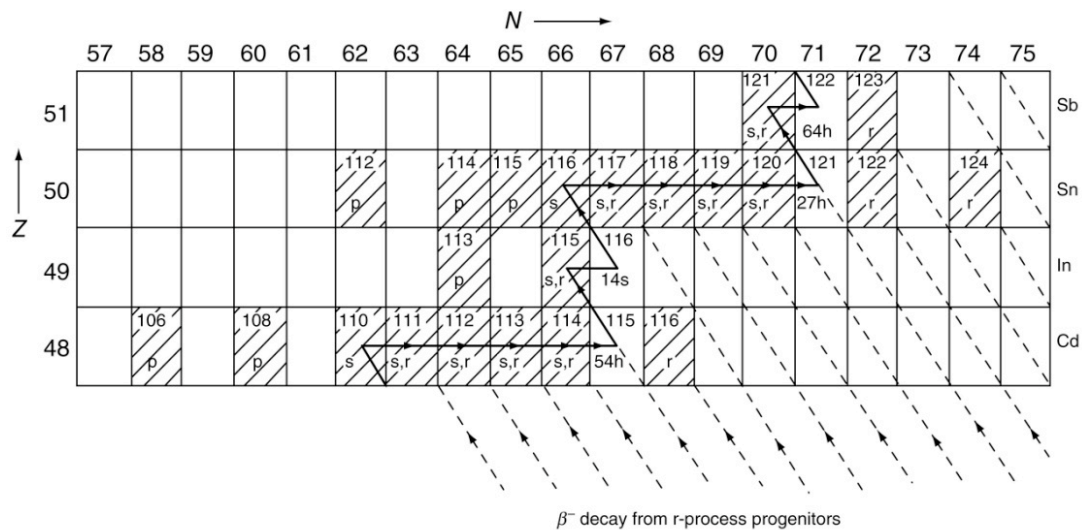

Figure 16.11: Nucleosynthesis of the elements Cd through to Sb. Stable isotopes are shown hatched. The solid line shows the path of the 'slow neutron capture' process. (Figure reproduced from Pearson, J.M. 1986, Nuclear Physics: Energy and Matter, Adam Hilger, Bristol).

Neutron-capture nucleosynthesis was already discussed in Lecture 7.5. The process of interest here is the 'rapid neutron capture', or r-process, whereby a nucleus can absorb several neutrons quickly before decaying. As the number of neutrons increases, the half-life of the isotope decreases until it is shorter than the interval between successive neutron captures, at which point the neutron-rich isotope will undergo β-decay.

For example, referring to Figure 16.11, if $^{115}_{49}$In nuclei absorb seven neutrons on timescales smaller than the half-lifes of the various isotopes along the way, $^{122}_{49}$In can be synthesised. If its half-life is short compared to the interval between successive neutron captures, then $^{122}_{49}$In will decay into $^{122}_{50}$Sn which, by definition, is then an r-process element. From Figure 16.11 it can be seen that some isotopes can be synthesised by both the s- and r-process.

16.5.1 Light Curves of Core Collapse Supernovae

The visible supernova explosion starts when the shock wave reaches the stellar surface, giving rise to a short pulse (~ 30 minutes) of soft X-ray emission. The luminosity then declines rapidly as the stellar surface expands and cools. When a massive H-rich envelope is present, the gas which was ionised by the shock enters a stage of prolonged recombination, releasing energy at a nearly constant temperature of ~ 5000 K; the photons emitted as the recombining electrons cascade down the H energy levels produce the plateau in the light curves of Type II-P SNe. In cases where the H-rich envelope is not sufficiently massive, the plateau phase is absent (Type II-L light curves).

The overall light curve on which the plateau is superposed in Type II-P SNe is due to the radioactive decay of isotopes produced by the shock front as it travels outwards through the star. As the shock wave moves through the Si layer, it raises the temperature to $T \sim 5 \times 10^9$ K; nuclear statistical equilibrium is reached in a few seconds, and explosive nucleosynthesis of Si takes place. As was the case with the slower hydrostatic burning stages prior to core collapse, Fe-group elements are produced, but the main product is $^{56}_{28}$Ni rather than $^{56}_{26}$Fe. The reason is that the timescale is too short for β-decays to take place and change the ratio of protons to neutrons. Since the 'fuel', $^{28}_{14}$Si, has Z/A = 1/2, (most of) the products also have

Z/A = 1/2, hence $^{56}_{28}$Ni instead of $^{56}_{26}$Fe. As the shock waves moves out and the temperature drops below $\sim 10^9$ K (around the O, Ne layer) explosive nucleosynthesis stops.

The most abundant isotope produced by explosive nucleosynthesis, $^{56}_{28}$Ni, is not stable but decays to $^{56}_{27}$Co via the β^+ decay reaction:

$$^{56}_{28}\text{Ni} \rightarrow ^{56}_{27}\text{Co} + e^+ + \nu_e + \gamma$$
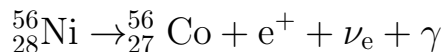
with a half-life $\tau_{1/2} = 6.1$ days.[1] $^{56}_{27}$Co subsequently decays to stable $^{56}_{26}$Fe by a similar reaction:

$$^{56}_{27}\text{Co} \rightarrow ^{56}_{26}\text{Fe} + e^+ + \nu_e + \gamma$$
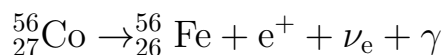
with the longer half-life $\tau_{1/2} = 77.7$ days. The high-energy photons produced by these decays power the emission from the expanding SN remnant.

Since radioactive decay is a statistical process, the rate of decay must be proportional to the number of atoms remaining in a sample (in this case the supernova remnant):

$$\frac{dN}{dt} = -\lambda N\,, \tag{16.8}$$

where λ is a constant. Integrating 16.8, we find:

$$N(t) = N_0\, e^{-\lambda t}\,, \tag{16.9}$$

where N_0 is the original number of radioactive atoms in the sample and $\lambda = \ln 2 / \tau_{1/2}$.

When radioactive decay is powering the SN light curve, the rate at which energy is deposited into the supernova remnant is proportional to the decay rate dN/dt. Thus, we have:

$$\frac{d \log_{10} L}{dt} = -\log_{10} e \cdot \lambda = -0.434\lambda \tag{16.10}$$

where L is the bolometric luminosity or, in terms of magnitudes:

$$\frac{d M_{\text{bol}}}{dt} = 1.086\lambda \tag{16.11}$$

---

[1] Recall the definition of half-life: if we take a sample of radioactive material initially consisting of X_0 atoms of isotope X, there is a 50% chance that any atom in the sample will decay to isotope Y over a time interval $\tau_{1/2}$. Thus, after a time $n \times \tau_{1/2}$ the fraction of isotope X remaining is $X/X_0 = 2^{-n}$.

In a typical Type II-P SN, the exponential decline of the light curve after 50–100 days reflects the decay of $^{56}_{27}$Co to $^{56}_{26}$Fe and implies that $\sim 0.07 M_\odot$ of $^{56}_{28}$Ni was ejected in the explosion. This puts constraints on the position of the 'mass cut' between the collapsing core and the ejected envelope (the remainder of the synthesised $^{56}_{28}$Ni is locked up in the collapsed compact object). This mass cut is a key parameter in computer calculations of the nucleosynthetic yields of supernovae. The light curves of Type Ib and Ic supernovae are completely dominated by the $^{56}_{28}$Ni $\rightarrow^{56}_{27}$ Co $\rightarrow^{56}_{26}$ Fe radioactive decay after the initial luminosity peak caused by shock breakout.

It is expected that the explosive nucleosynthesis of the supernova shock also produces significant amounts of other radioactive isotopes, such as $^{57}_{27}$Co, with a half-life $\tau_{1/2} = 271$ days; $^{22}_{11}$Na ($\tau_{1/2} = 2.6$ years) and $^{44}_{22}$Ti ($\tau_{1/2} \simeq 47$ years). If these isotopes are present in sufficient quantities, each in turn may contribute to the overall light curve, causing the slope of the curve to change with time (see Figure 16.12).
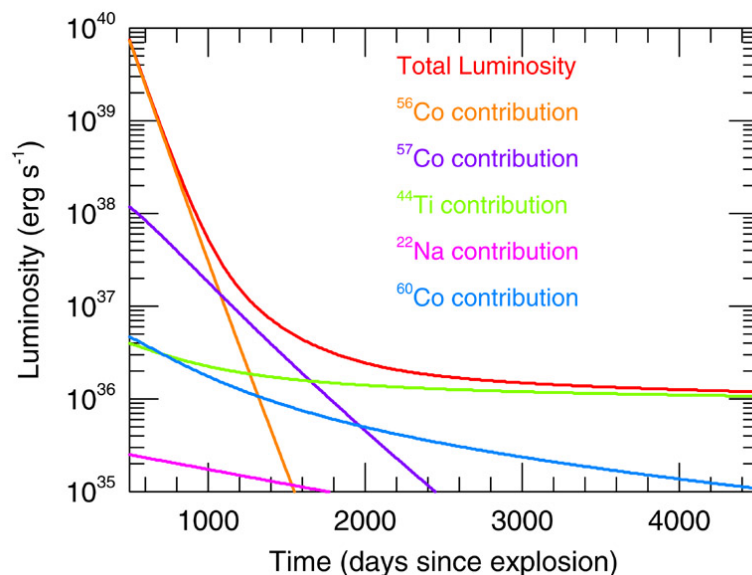

Figure 16.12: Radioactive decays contributing to supernova light curves. (Reproduced from http://cococubed.asu.edu, Frank Timmes's webpages at Arizona State University).

16.6   SN1987A in the Large Magellanic Cloud

The closest supernova in modern times was SN1987A in the Large Magellanic Cloud, our companion galaxy at a distance of 50 kpc. Being so close, this event was studied (and continues to be so) in more detail and

with higher precision than any other supernova. The huge amount of data acquired on this object confirmed some of the theoretical ideas on core-collapse SNe but also improved our understanding of such events by presenting us with a number of surprises.

16.6.1   Neutrinos

Arguably the most exciting observation of SN1987A was the detection of its neutrinos—the first time that neutrinos had been detected from an astronomical source other than the Sun, validating the basic picture of the formation of a neutron star from a collapsed iron core.

A total of 20 electron anti-neutrinos were detected simultaneously in the span of 12.5 seconds by two underground Cerenkov experiments (designed to search for proton decay), one in Japan and the other in the USA. The typical energies of the $\bar{\nu}_e$ were $\sim 20\,\text{MeV}$. Neutrinos hardly interact with ordinary matter. Correcting for the very low detection efficiency, implies that a time-integrated flux, or fluence, of $2 \times 10^9\,\text{cm}^{-2}$ $\bar{\nu}_e$ particles had reached the Earth. Further correcting for the other five types of neutrinos $(\nu_e, \nu_\mu, \bar{\nu}_\mu, \nu_\tau$ and $\bar{\nu}_\tau)$ and for the surface of a sphere of radius $50\,\text{kpc}$, we find that the total energy of the neutrinos emitted by SN1987A was:

$$E_\nu \simeq 2 \times 10^9\,\text{cm}^{-2} \times 6 \times \left(20\,\text{Mev} \times 1.6 \times 10^{-6}\,\text{erg}\,\text{MeV}^{-1}\right)$$
$$\times 4\pi \left(5 \times 10^4 \text{pc} \times 3.1 \times 10^{18}\text{cm}\,\text{pc}^{-1}\right)^2$$
$$\simeq 10^{53}\,\text{erg}$$

close to the total energy expected from the collapse of a stellar core with the parameters given in Section 16.4.1.

The neutrinos from SN1987A were detected on February 23.31 UT, three hours *before* the arrival of the first photons from the optical event. The neutrinos began their trip to Earth ahead of the photons, presumably because the exploding star became optically thin to neutrinos before the shock wave reached the surface. To keep ahead of the photons over the 163 000 light-years distance from the LMC to Earth, the neutrinos must have travelled close to the speed of light. This conclusion, together with lack of significant dispersion in the arrival times of neutrinos of different energies, has been used to place an upper limit to the mass of the electron neutrino $m_{\nu_e} \leq 16\,\text{eV}$, consistent with the upper limit of $2.2\,\text{eV}$ from

the most sensitive laboratory experiments. Here is a good example of an interface between astronomy and particle physics.

16.6.2   The Progenitor of SN1987A

With so many images of the LMC obtained at many ground-based observatories over the years, it was relatively straightforward to identify the progenitor on pre-explosion photographic plates as a 12th-mag star previously catalogued as $\mathrm{Sk}-69\,202$ (see Figure 16.13).
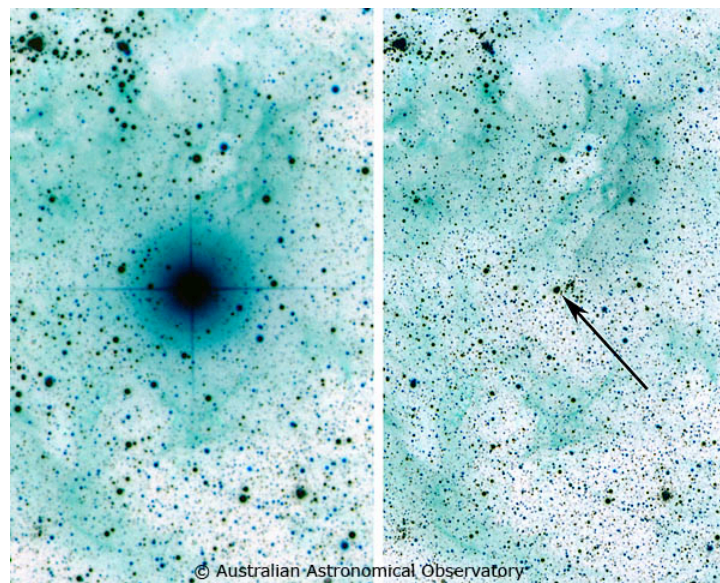

Figure 16.13: SN1987A in the Large Magellanic Cloud. (Photos by David Malin, Anglo-Australian Observatory).

Surprisingly, $\mathrm{Sk}-69\,202$ was a *blue*, rather than red, supergiant, classified as B3 I, with $L \approx 1.1 \times 10^5 L_\odot$, $T_{\mathrm{eff}} \approx 16\,000\,\mathrm{K}$ and probable initial mass $M_{\mathrm{ZAMS}} \approx 18 M_\odot$. This quickly led people to reconsider models of stellar evolution for massive stars and to realise the perhaps previously unappreciated importance of metallicity in shaping their evolution. The LMC has a present-day metallicity $Z_{\mathrm{LMC}} \approx 1/2 Z_\odot$. Even a modest factor of two drop in metallicity has several consequences: it results in an extended 'blue loop' in the path in the H-R diagram taken by an evolving massive star (see Figure 16.14); it reduces the amount of mass loss through the stellar wind (as we saw in Lecture 15); and the star has a hotter photosphere.
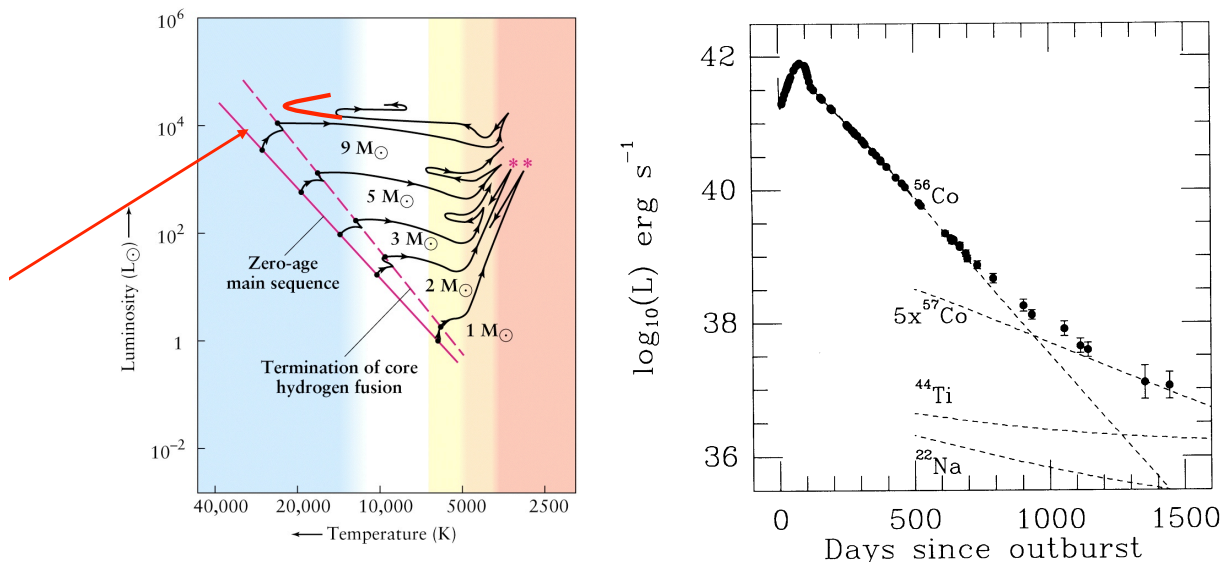
Figure 16.14: *Left:* At low metallicities, massive stars exhibit more extended 'blue loops' in the upper regions of the H-R diagram. This probably explains why the progenitor of SN1987A exploded when it was a blue, rather than red, supergiant. *Right:* Bolometric light curve of SN1987A through the first 1444 days after the explosion. The dashed lines show the contributions from radioactive isotopes produced by explosive nucleosynthesis. (Figure reproduced from Carroll & Ostlie, *Modern Astrophysics*; original data from Suntzeff et al. 1992, ApJ, 384, L33).

16.6.3 The Light Curve

The right panel of Figure 16.14 shows the light curve of SN1987A from photometric observations carried out during four years after the explosion. Not immediately evident from this figure is the subluminous nature of this supernova—whereas typical Type II SNe reach $M_{\rm bol} = -18$, SN1987A peaked at $M_{\rm bol} = -15.5$, ten times fainter. Also, its rise to maximum light was much slower than normal, the rising portion of the light curve lasting for 80 days.

These 'anomalies' go hand-in-hand with the fact that the star exploded as a blue supergiant, much smaller and denser than a red supergiant. Consequently, a larger fraction of the thermal energy released in the collapse was converted into the mechanical energy required to lift the envelope of the star out of the deeper potential well of a blue supergiant.

The proximity of SN1987A allowed us to follow its light curve for longer, and more accurately, than is normally possible for other supernovae. The change in slope as the decay of $^{57}_{27}$Co takes over from $^{56}_{27}$Co near day 1000 is evident from Figure 16.14. An independent confirmation of our ideas of radioactive powering of the light curve was the direct detection in late

1987 of the γ-ray emission lines at $847\,\mathrm{keV}$ and $1238\,\mathrm{keV}$ that accompany the decay of $^{56}_{27}\mathrm{Co}$ to $^{56}_{26}\mathrm{Fe}$. These emission lines were recognised in accumulated spectra recorded by the NASA Solar Maximum Mission satellite (Matz et al. 1988, Nature, 331, 416). These observations showed that about $0.075 M_\odot$ of $^{56}_{28}\mathrm{Ni}$, the parent nucleus of $^{56}_{27}\mathrm{Co}$, was formed in the explosion. Later, the $122\,\mathrm{keV}$ emission line from $^{57}_{27}\mathrm{Co}$ was observed in 1991 by the *Compton Gamma Ray Observatory*, and $0.003 M_\odot$ of this nuclide was inferred to have been synthesised.

16.6.4 The Supernova Remnant

While the progenitor of SN1987A experienced a reduced amount of mass loss compared with a more metal-rich star of the same mass, we have direct confirmation of pre-explosion episodes of mass loss in the appearance of the supernova remnant, recorded with an exquisite series of images by the *Hubble Space Telescope* (Figure 16.15).

The radioactive debris of SN1987A, expanding with velocities of up to several thousand km s^{-1}, is at the centre of a triple ring system; this is circumstellar gas which was probably dark before the SN and was heated and ionized by the flash of radiation at the time of shock breakout. The

Figure 16.15: Images of SN1987A and its immediate surroundings recorded with the *Hubble Space Telescope* on 6 February 1996 (*Left*) and 6 December 2006 (*Right*). The inner ring has been brightening in clumps as the shock front from the supernova began colliding with the slower moving material ejected by the SN progenitor during its red supergiant phase.

inner ring exhibits an enhanced abundance of nitrogen (by a factor of 10 compared with the interstellar abundance of N in the LMC) implying that it has been through the CNO nuclear burning process, and is expanding with a velocity $v_{\exp} = 10\,\mathrm{km\,s^{-1}}$; both findings strongly point to an origin in a mass loss event during an earlier red supergiant phase. The radius of the inner ring (which is circular but appears elliptical because it is inclined to our line of sight) is $\sim 0.2\,\mathrm{pc}$; combined with its velocity, it implies that this gas was ejected $\sim 20,000$ years before the SN explosion.

Models of the ring structure require the density of the slow wind in the equatorial plane be 20 times the density of the wind in the polar direction. The reason for such an aspherical, but axisymmetric, wind remains unclear, although similar structures are inferred to exist in planetary nebulae. One possibility is that a binary companion was involved in the equatorial mass loss. There is no direct evidence for a binary companion, although such a model may be attractive on other grounds, including mixing of the progenitor- star envelope and even the blueward evolution of the star before the explosion.

The shock front from the expanding supernova remnant began to collide with the slower moving stellar wind comprising the inner ring in 1996. The result was a brilliant display of bright clumps in the inner ring that developed over the next several years (right panel of Figure 16.15). The two larger rings are not in planes containing the central explosion, but lie in front of and behind the star. Their origin is still unclear. While several models have been put forward, involving a binary companion and/or a fast blue supergiant wind, they generally seem somewhat contrived and there is no general consensus as to the interpretation of these enigmatic features.

16.6.5   The Light Echo of SN1987A

In 1939, the French astronomer Paul Couderc developed the basic mathematical description of light echoes and applied it to earlier observations of Nova Persei 1901. Soon after the explosion, Roger Chevalier and others predicted that SN1987A should give rise to very conspicuous light echoes, first detected a year after the explosion and monitored over several years, as shown in Figure 16.16.
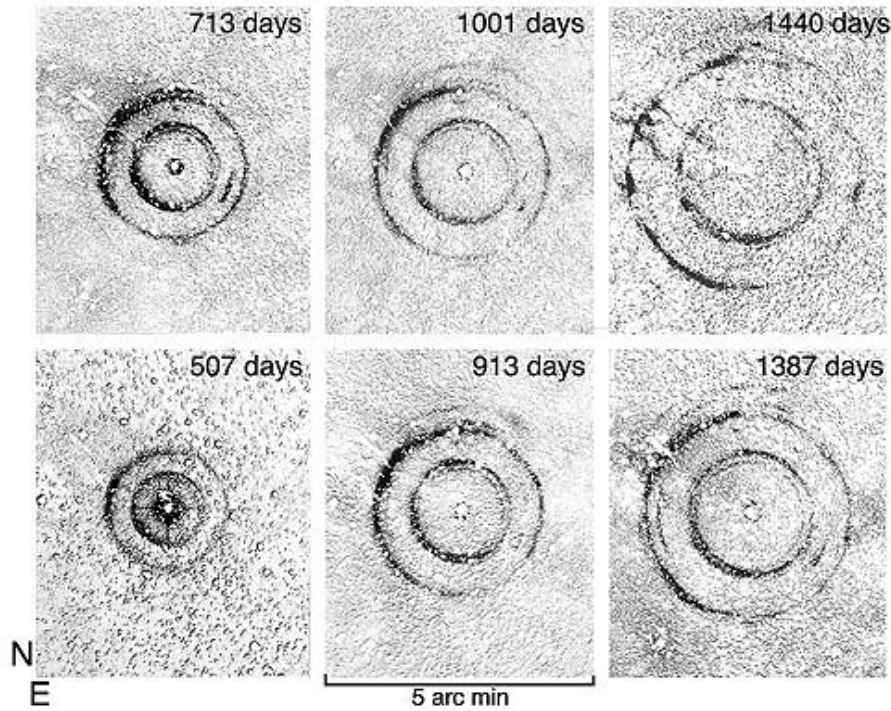
Figure 16.16: Scattered light echoes from SN1987A photographed with the Anglo-Australian Telescope.

The formation of the light echoes is illustrated in Figure 16.17. At any one time after the explosion, there is an ellipsoidal surface of equal delay in light-travel time. If mirrors were placed on such a surface, we would see reflected light from the supernova. In an astronomical situation, the 'mirrors' are dust particles which scatter the incident starlight; if the dust is located in planar sheets, we see rings where the sheets intersect the light-travel time delay ellipse. By modelling the rings produced by SN1987A
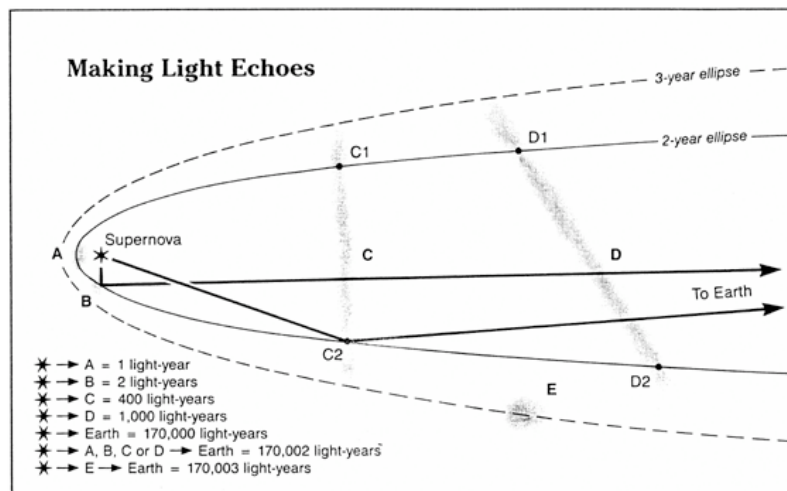

Figure 16.17: Schematic diagram of light echoes from SN1987A (not to scale).

24

and their evolution, Chevalier and collaborators showed that they occur in sheets of dust (and gas) located ~ 120 and $\sim 330\,\mathrm{pc}$ in front of the supernova, and that the dust producing the light echoes is comparable to the total column density of dust in front of the stars in this region of the LMC. The two main concentrations of interstellar material in this general direction are also seen in the absorption lines they produce in the spectra of background stars. The changing detail of the light echoes is a vivid demonstration of the small-scale structure if the interstellar medium, which had perhaps not been fully appreciated before.

16.7   Gamma-ray Bursts

We conclude this lecture with a brief mention of γ-ray bursts (GRBs) which, at least in some cases, appear to be associated with the core-collapse of massive stars.

About once a day, at some random location in the sky, a shower of γ-ray photons with energies between $1\,\mathrm{keV}$ and many GeV appears. The bursts last from 1/100 to 1000s of seconds, have rise times as fast at 10^{-4} seconds followed by an exponential decay. After 25 years of controversy, GRB events were finally identified as being extragalactic. This realisation also implied that GRBs are by far the most energetic astrophysical sources known; even allowing for the fact that the radiation is highly beamed, at peak GRBs can be three order of magnitude more luminous than the most luminous QSOs and 10^7 times brighter than the most luminous SNe!

After thousands of catalogued events, it is clear that there are two basic classes of GRBs: events that last less than $2\,\mathrm{s}$ are short-hard events, while those that last longer than $2\,\mathrm{s}$ are long-soft GRBs (the 'hard' and 'soft' labels refer to the spectral energy distribution—a hard spectrum source has more energy at higher energies and shorter wavelengths). Short bursts are thought to be associated with mergers of compact objects—neutron star-neutron star or neutron star-black hole mergers. Long-duration GRBs are thought the accompany the core collapse of very massive stars under the 'right' circumstances.

In the 'collapsar' model developed by Stan Woosley and collaborators at the University of California, Santa Cruz, a progenitor star with sufficiently

high mass (possibly a Wolf-Rayet star) collapses to form a black hole. If the star is rotating, matter would fall freely along the rotation axis onto the black hole on timescales of seconds; however, along the equatorial plane infalling matter would be held up in an accretion disk by a centripetal force. Detailed numerical simulations indicate that after a few seconds the polar regions become sufficiently evacuated of matter to allow the deposited gravitational energy to begin to propagate outwards, forming a relativistic and highly collimated jet. The jet is thought to carry enough energy that, even if only a small fraction couples to the matter in the jet boundary, it will be enough to explode the star.

Empirical confirmation of this scenario was provided by the detection in 1998 of GRB 980425 phenomenologically connected to SN1998bw, a hyper-luminous Type Ib SN with very broad spectral lines (a Type Ib-BL SN), indicative of outflows with speeds $v_{\mathrm{ej}} \gtrsim 0.1c$. Tens of more cases are now known where a Type Ib SN has been found to be associated with a long-duration GRB event.

Most GRB events occur at redshifts which are too high to discern an associated supernova (which has to be separated from the light of the GRB afterglow and of the host galaxy). However, there are also a few cases, at
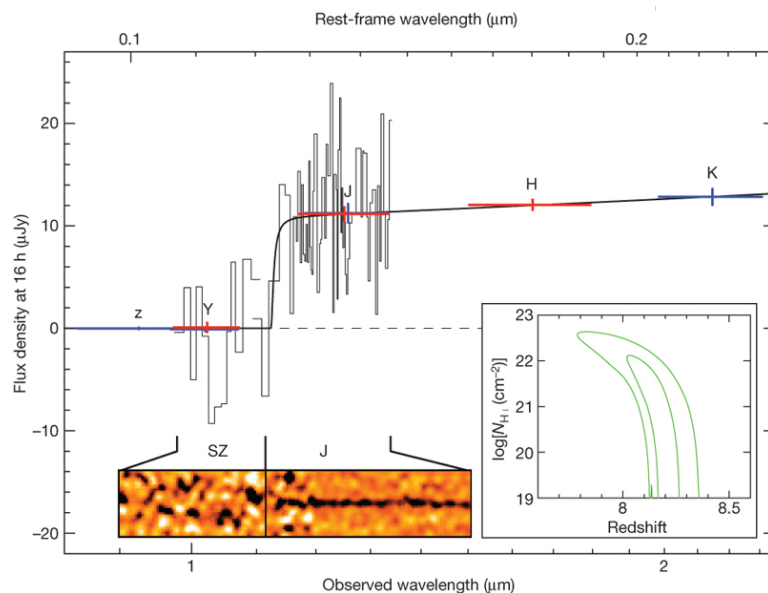

Figure 16.18: Near-IR spectrum and photometry of GRB 090423 at $z \simeq 8.2$, reproduced from Tanvir et al. 2009, Nature, 461, 1254. The inset shows the 1σ and 2σ confidence contours on the correlated values of redshift and absorbing H I column density in the host galaxy.

lower redshifts, where a conventional SN should have been detected—had it occurred—but it wasn't. Perhaps these are the 'failed SNe' of Woosley's original (i.e. pre-GRB) collapsar model, although opinions are still divided.

The extreme brightness of GRBs, albeit for only brief periods, makes them visible out to cosmological distances. Indeed, one of the highest redshift objects known is the host galaxy of GRB 090423 at $z \simeq 8.2$, only $600\,\text{Myr}$ ($\sim 5\%$ of the present age of the Universe) after the Big Bang (see Figure 16.18). Thus, GRBs can be some of the best probes of the earliest star formation episodes in the Universe. Furthermore, the act as bright background light sources in whose spectrum we can see the absorption produced by intervening material in galaxies and in the intergalactic medium over very long sight-lines (see Figure 16.19). With the technique of absorption-line spectroscopy, astronomers have used GRBs to study the properties of the Universe at different stages of its evolution, from its infancy to the present day.
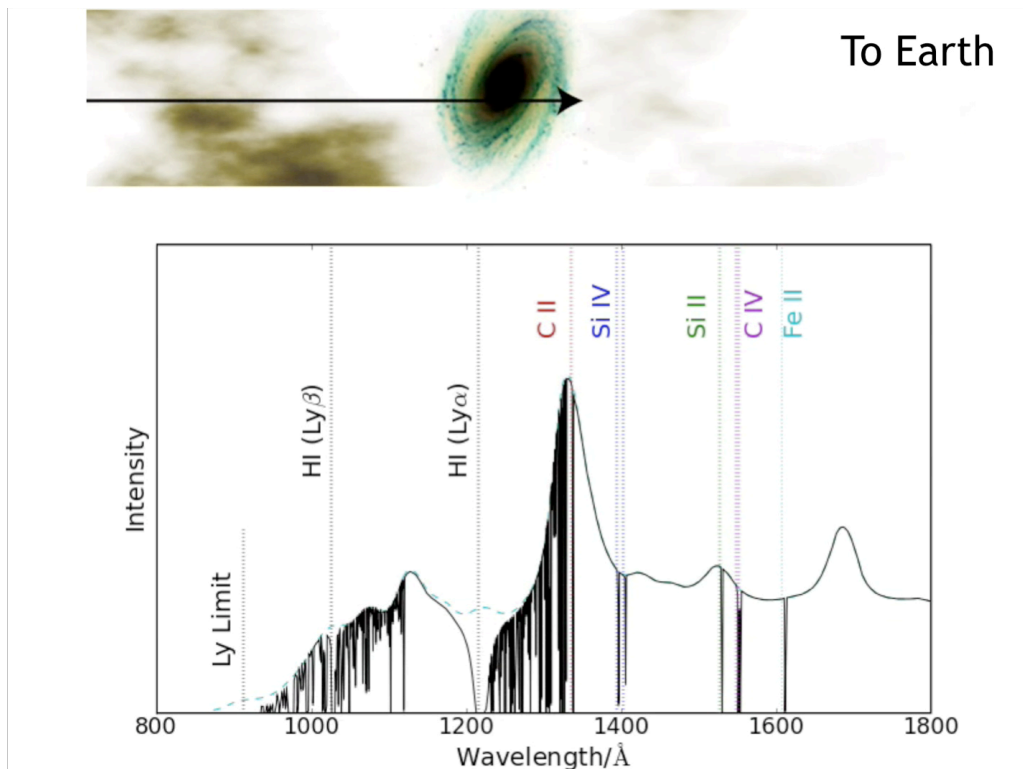

Figure 16.19: Absorption line spectroscopy of bright GRB afterglows can provide detailed physical information on intervening gas in and between galaxies fortuitously located along the line of sight. (Figure courtesy of Andrew Pontzen).